IEEE TRANSACTIONS ON

# GEOSCIENCE AND REMOTE SENSING

A PUBLICATION OF THE IEEE GEOSCIENCE AND REMOTE SENSING SOCIETY

AUGUST 2008 VOLUME 46 NUMBER 8 IGRSD2 (ISSN 0196-2892)

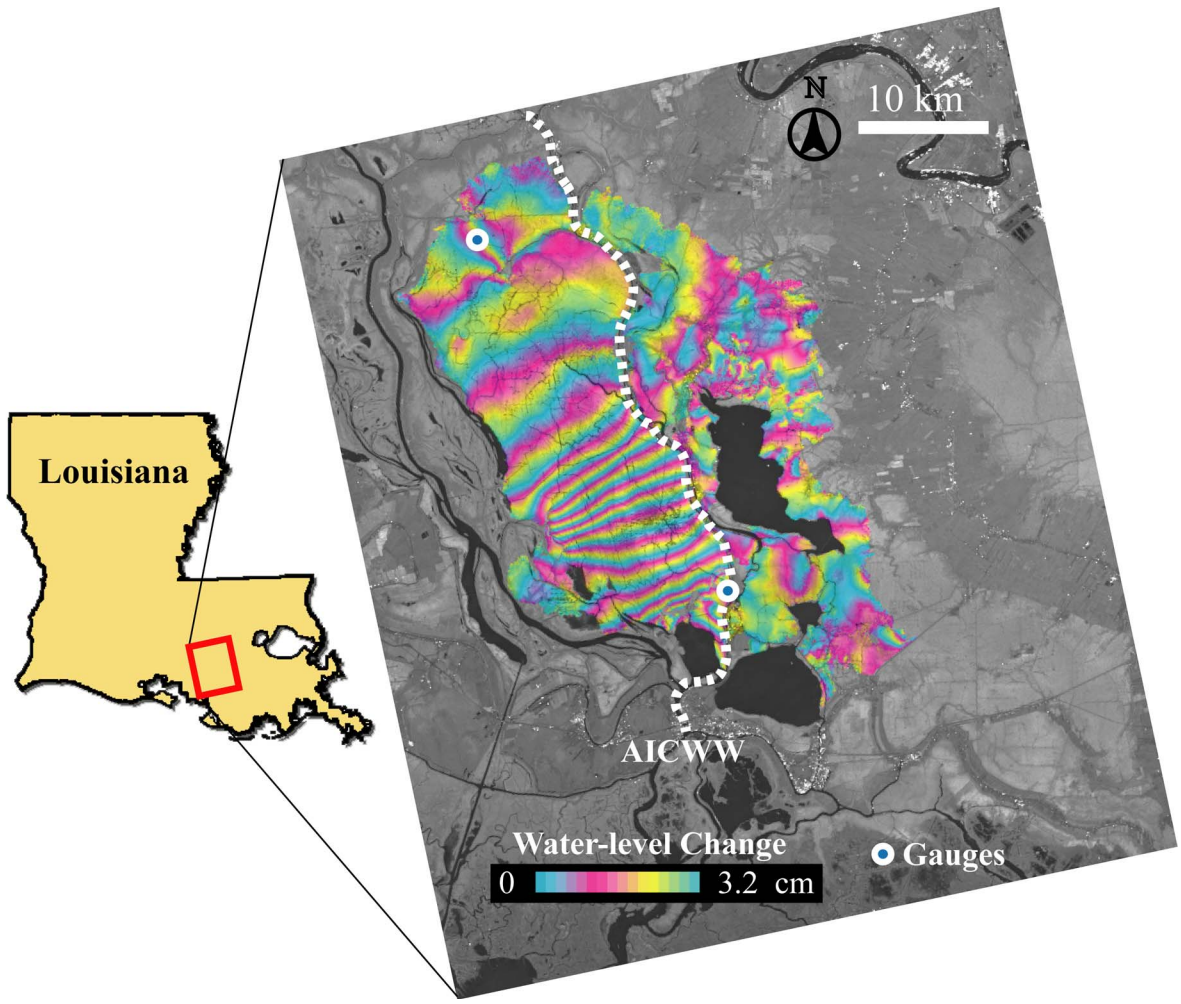


C-band Radarsat-1 InSAR image shows water-level changes over the swamp forest in southeastern Louisiana between May 22 and June 15, 2003. InSAR-derived water-level changes at the selected locations are compared with gauge readings.

IEEE

IEEE TRANSACTIONS ON

# GEOSCIENCE AND REMOTE SENSING

A PUBLICATION OF THE IEEE GEOSCIENCE AND REMOTE SENSING SOCIETY

AUGUST 2008 VOLUME 46 NUMBER 8 IGRSD2 (ISSN 0196-2892)

PAPERS

**Radar**

Radarsat-1 and ERS InSAR Analysis Over Southeastern Coastal Louisiana: Implications for Mapping Water-Level Changes Beneath Swamp Forests . . . *Z. Lu and O. Kwoun* 2167

Information Theory-Based Approach for Contrast Analysis in Polarimetric and/or Interferometric SAR Images . . . *J. Morio, P. Réfrégier, F. Goudail, P. C. Dubois-Fernandez, and X. Dupuis* 2185

Sea Ice Deformation State From Synthetic Aperture Radar Imagery—Part II: Effects of Spatial Resolution and Noise Level . . . *W. Dierking and J. Dall* 2197

Squint Spotlight SAR Raw Signal Simulation in the Frequency Domain Using Optical Principles . . . *Y. Wang, Z. Zhang, and Y. Deng* 2208

A Two-Dimensional Spectrum Model for General Bistatic SAR . . . *X. Geng, H. Yan, and Y. Wang* 2216

An Omega-K Algorithm With Phase Error Compensation for Bistatic SAR of a Translational Invariant Case . . . *X. Qiu, D. Hu, and C. Ding* 2224

Imaging Simulation of Bistatic Synthetic Aperture Radar and Its Polarimetric Analysis . . . *F. Xu and Y.-Q. Jin* 2233

A Multistatic GNSS Synthetic Aperture Radar for Surface Characterization . . . *T. Lindgren and D. M. Akos* 2249

**Subsurface and Geophysical Signal Processing**

The Detection of Buried Pipes From Time-of-Flight Radar Data . . . *G. Borgioli, L. Capineri, P. Falorni, S. Matucci, and C. G. Windsor* 2254

Determination of Bathymetric and Current Maps by the Method DiSC Based on the Analysis of Nautical X-Band Radar Image Sequences of the Sea Surface (November 2007) . . . *C. M. Senet, J. Seemann, S. Flampouris, and F. Ziemer* 2267

Automatic $P$-Phase Picking Based on Local-Maxima Distribution . . . *C. Panagiotakis, E. Kokinou, and F. Vallianatos* 2280

**Radiometry and Atmospheric Measurements**

Efficient Model-Based Estimation of Atmospheric Transmittance and Ocean Wind Vectors From WindSat Data . . . *D.-J. Kim and D. R. Lyzenga* 2288

Surface Emissivity of Arctic Sea Ice at AMSU Window Frequencies . . . *N. Mathew, G. Heygster, C. Melsheimer, and L. Kaleschke* 2298

Improved Retrieval of Total Water Vapor Over Polar Regions From AMSU-B Microwave Radiometer Data . . . *C. Melsheimer and G. Heygster* 2307

The Fully Polarimetric Imaging Radiometer SPIRA at 91 GHz . . . *A. Đurić, A. Magun, A. Murk, C. Mätzler, and N. Kämpfer* 2323

Side-Face Effect of a Dielectric Strip on Its Optical Properties . . . *W. Sun, B. Lin, Y. Hu, Z. Wang, Y. Fu, Q. Feng, and P. Yang* 2337

*(Contents Continued on Page 2166)*

IEEE

*(Contents Continued from Page 2165)*

Normalized Differential Spectral Attenuation (NDSA) Measurements Between Two LEO Satellites: Performance Analysis in the Ku/K-Bands . . . . . *L. Facheris, F. Cuccoli, and F. Argenti* 2345
Whitening Dual-Polarized Weather Radar Signals With a Hermitian Transformation . . . . . *E. Hefner and V. Chandrasekar* 2357

**Soil Moisture and Temperature**

Soil Moisture Retrieval During a Corn Growth Cycle Using L-Band (1.6 GHz) Radar Observations . . . . . *A. T. Joseph, R. van der Velde, P. E. O'Neill, R. H. Lang, and T. Gish* 2365
Vertical Resolution Estimates in Version 5 of AIRS Operational Retrievals. . . . . *E. S. Maddy and C. D. Barnet* 2375

**Information Processing**

Three-Dimensional Motion Estimation of Atmospheric Layers From Image Sequences . . . . . *P. Héas and E. Mémin* 2385
Medium Spatial Resolution Satellite Imagery for Estimating and Mapping Urban Impervious Surfaces Using LSMA and ANN . . . . . *Q. Weng and X. Hu* 2397
Improvement of Target Detection Methods by Multiway Filtering . . . . . *N. Renard and S. Bourennane* 2407
Multiscale Representation and Segmentation of Hyperspectral Imagery Using Geometric Partial Differential Equations and Algebraic Multigrid Methods . . . . *J. M. Duarte-Carvajalino, G. Sapiro, M. Vélez-Reyes, and P. E. Castillo* 2418
Hyperspectral Subspace Identification . . . . . *J. M. Bioucas-Dias and J. M. P. Nascimento* 2435
A Genetic-Programming-Based Method for Hyperspectral Data Information Extraction: Agricultural Applications . . . . . *C. Chion, J.-A. Landry, and L. Da Costa* 2446

ANNOUNCEMENTS

Call for Papers—IEEE TRANSACTIONS ON GEOSCIENCE AND REMOTE SENSING Special Issue on Calibration and Validation of ALOS Sensors (PALSAR, AVNIR-2, and PRISM) and Their Use for BIO- and Geophysical Parameter Retrievals . . . . . 2458
Call for Papers—IEEE TRANSACTIONS ON GEOSCIENCE AND REMOTE SENSING Special Issue on the IEEE 2008 International Geoscience and Remote Sensing Symposium (IGARSS 2008) . . . . . 2459
Call for Papers—IEEE TRANSACTIONS ON GEOSCIENCE AND REMOTE SENSING Special Issue on the 10th Specialist Meeting on Microwave Radiometry and Remote Sensing of the Environment (MICRORAD 2008) . . . . . 2460

About the Cover: C-band Radarsat-1 InSAR image (May 22–June 15, 2003) is capable of mapping water-level changes of coastal wetlands over southeastern Louisiana. The InSAR image suggests that water-level changes are dynamic and spatially heterogeneous, and are disconnected by structures and barriers. Water-level changes over the swamp forest west of the Atchafalaya Intracoastal Waterway (AICWW) are different from those east of AICWW, and neither cannot be represented by readings from sparsely distributed gauge stations along the AICWW. For more information, please see ''Radarsat-1 and ERS InSAR Analysis Over Southeastern Coastal Louisiana: Implications for Mapping Water-Level Changes Beneath Swamp Forests,'' by Lu and Kwoun, which begins on page 2167.

# Radarsat-1 and ERS InSAR Analysis Over Southeastern Coastal Louisiana: Implications for Mapping Water-Level Changes Beneath Swamp Forests

Zhong Lu, *Senior Member, IEEE*, and Oh-ig Kwoun

***Abstract*—Detailed analysis of C-band European Remote Sensing 1 and 2 (ERS-1/ERS-2) and Radarsat-1 interferometric synthetic aperture radar (InSAR) imagery was conducted to study water-level changes of coastal wetlands of southeastern Louisiana. Radar backscattering and InSAR coherence suggest that the dominant radar backscattering mechanism for swamp forest and saline marsh is double-bounce backscattering, implying that InSAR images can be used to estimate water-level changes with unprecedented spatial details. On the one hand, InSAR images suggest that water-level changes over the study site can be dynamic and spatially heterogeneous and cannot be represented by readings from sparsely distributed gauge stations. On the other hand, InSAR phase measurements are disconnected by structures and other barriers and require absolute water-level measurements from gauge stations or other sources to convert InSAR phase values to absolute water-level changes.**

***Index Terms*—Forestry, hydrology, interferometry, scattering, synthetic aperture radar (SAR), vegetation, water.**

## I. Introduction

WETLANDS cover more than 4% of the Earth's land surface and include hydrologic and other processes that are fundamental to understanding ecological and climatic changes [1]–[4]. Measurement of changes in water level over wetlands and, consequently, of changes in water-storage capacity, provides a governing parameter in hydrologic models and is required for comprehensive assessment of flood hazards [5]. Inaccurate knowledge of floodplain storage capacity in wetlands can lead to significant errors in hydrologic simulation and modeling. *In situ* measurement of water levels over wetlands is cost-prohibitive, and insufficient coverage of stage recording instruments results in poorly constrained estimates of the water-storage capacity of wetlands. With frequent coverage over wide areas, satellite sensors may provide a cost-effective tool for accurate measurements of water storage.

Synthetic aperture radar (SAR) is an active microwave sensor with all-weather day and night operational imaging capability. The amplitude (or intensity) of the SAR backscattering signal is sensitive to terrain slope, surface roughness, and dielectric constant, and has been used in characterizing wetland types, conditions, and flooding [6]–[10]. The phase of the SAR backscattering signal is related to the apparent distance from the satellite to ground resolution elements as well as the interaction between radar waves and scatterers within a resolution element of the imaged area.

Interferometric SAR (InSAR) combines phase information to produce an interferogram from two or more radar images of the same area acquired from similar vantage points at different times. The interferogram depicts range changes between the radar and the ground, and can be further processed with a digital elevation model (DEM) to produce an image of ground deformation at a horizontal resolution of tens of meters over areas of $\sim$100 km $\times$ 100 km, with centimeter to subcentimeter vertical precision under favorable conditions [11], [12].

Alsdorf *et al.* [13], [14] found that interferometric analysis of L-band (wavelength of $\sim$24 cm) Shuttle Imaging Radar-C and Japanese Earth Resources Satellite (JERS-1) SAR imagery can yield centimeter-scale measurements of water-level changes throughout inundated floodplain vegetation. Their work confirmed that scattering elements for L-band radar consist primarily of the water surface and vegetation trunks, which allows double-bounce backscattering returns (i.e., the radar signal is initially reflected away from the sensor by the water's surface, toward a tree bole or other vertical structure and is then directly reflected toward the sensor). Later, Wdowinski *et al.* [15] applied L-band JERS-1 images to study water-level changes over the Everglades in Florida. All of these studies rely on this common understanding: Flooded forests permit double-bounce returns of L-band radar pulses, thus allowing InSAR coherence (a parameter quantifying the degree of changes in backscattering characteristics) to be maintained for monitoring changes in the height of the water surface.

Manuscript received July 9, 2007; revised December 7, 2007. This work was supported in part by the U.S. Geological Survey (USGS) under Contract O3CRCN0001 Director Venture Capital Fund, by the USGS Eastern Region Venture Capital Fund, by the USGS Land Remote Sensing Program, and by the NASA Solid Earth and Natural Hazards Program (SENH-0000-0229).

Z. Lu is with the U.S. Geological Survey, Earth Resources Observation and Science Center and Cascades Volcano Observatory, Vancouver, WA 98683 USA (e-mail: lu@usgs.gov).

O. Kwoun is with the Science Applications International Corporation, contractor to the U.S. Geological Survey Center for Earth Resources Observation and Science, Sioux Falls, SD 57198 USA (e-mail: okwoun@usgs.gov).

Digital Object Identifier 10.1109/TGRS.2008.917271

0196-2892/$25.00 © 2008 IEEE

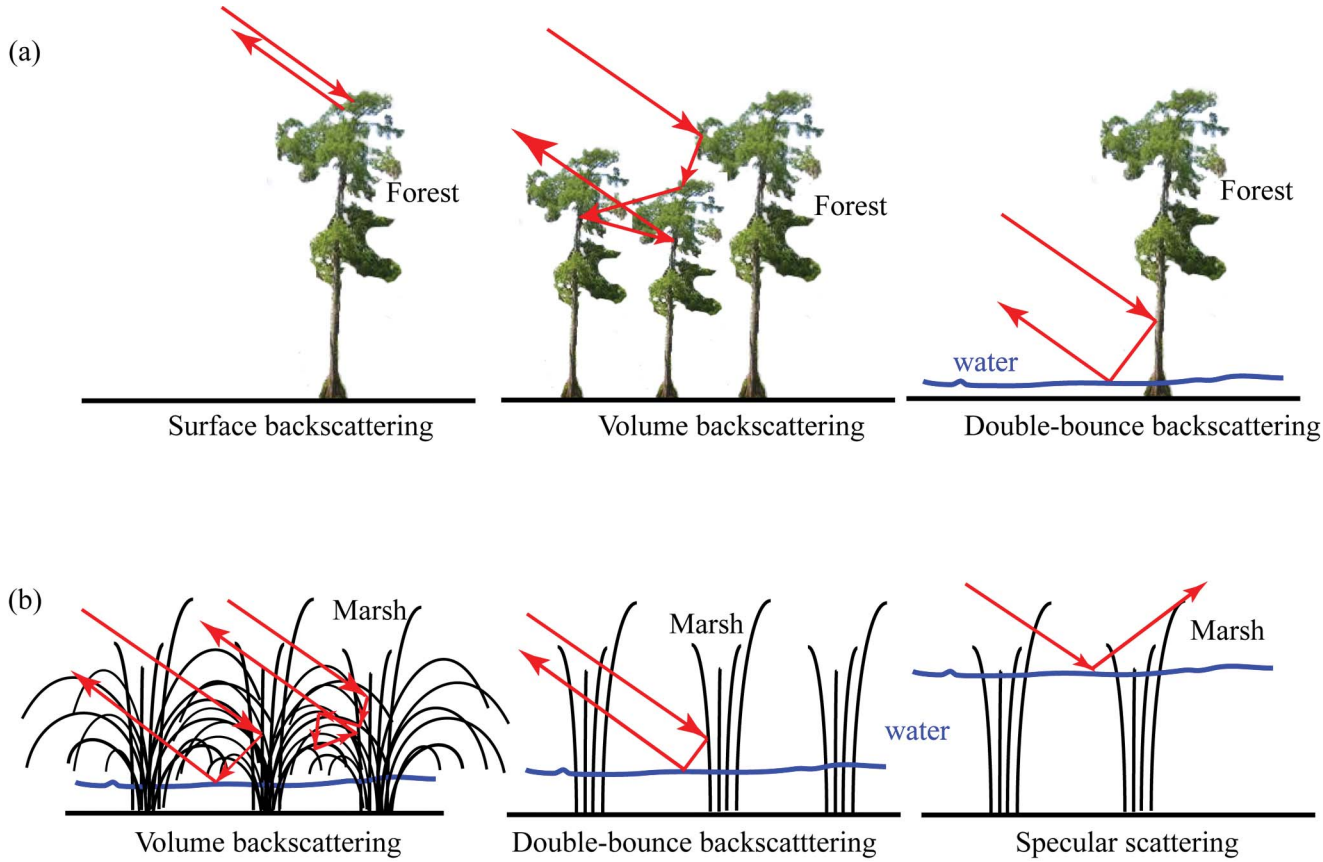


Fig. 1. Schematic figures showing the contributions of radar backscattering over (a) forests and (b) marshes due to canopy surface backscattering, canopy volume backscattering, specular scattering, and double-bounce backscattering.

Using a few C-band (VV polarization) SAR images from European Remote Sensing 1 and 2 (ERS-1/ERS-2) satellites, Lu *et al.* [16] reported that the InSAR images maintained adequate coherence to measure phase change over swamp forests in southeastern Louisiana. This finding was unexpected because the radar signal with shorter wavelength than L-band, such as C-band (wavelength of 5.66 cm), was thought to backscatter from the upper canopy of swamp forests rather than the underlying water surface, and a double-bounce travel path could only occur over inundated macrophytes and small shrubs [17]–[20]. The study by Lu *et al.* [16] suggested that the swamp forests composed of moderately dense trees with a medium-low canopy closure (i.e., 20%–50% tree cover) could maintain good coherence to allow measurement of water-level changes from C-band interferometric phase observations. The authors showed that the coherence of C-band interferograms could be maintained over swamp forests for more than three to five years.

In this paper, we have expanded the work by Lu *et al.* [16] to further quantify the water-level changes from C-band InSAR measurements using both vertical-transmit and vertical-receive (VV) polarized ERS-1/ERS-2 and horizontal-transmit and horizontal-receive (HH) polarized Radarsat-1 images. After laying out the framework for measuring water-level changes using InSAR phase measurements, we systematically analyze the interferometric coherence measurements for different vegetation types, seasonality, and time separation. We then study the InSAR-derived water-level changes over swamp forests. Finally, we discuss the potentials and challenges of measuring water-level changes over swamp forests from InSAR imagery.

## II. Mapping Water-Level Changes by InSAR

Interactions of C-band radar waves with water surface are relatively simple [21]. As SAR transmits radar pulses at an off-nadir look angle, a smooth open-water surface causes most of the radar energy to reflect away from the radar sensor, resulting in little energy being returned back to the SAR receiver. When the open-water surface is rough and turbulent, part of the radar energy can be scattered back to the sensor; however, the SAR signals over open water are not coherent if two radar images are acquired at different times. Thus, it has been generally accepted that InSAR is an inappropriate tool to use in studying changes in the water level of open water.

Interactions of C-band radar waves with wetlands can be complex [22]. Over flooded vegetation, the radar backscattering consists of contributions from the interactions of radar waves with the canopy surface, canopy volume, and water surface. Based on the canopy backscattering model for continuous tree canopies developed by Sun [23], we can infer that the total radar backscattering over wetland can be approximated as the incoherent summation of contributions from the following: 1) canopy surface backscattering; 2) canopy volume backscattering that includes backscattering from multiple path

interactions of canopy water; and 3) double-bounce trunk-water backscattering [Fig. 1(a)]. The relative contributions from surface backscattering, volume backscattering, and double-bounce backscattering are controlled primarily by vegetation type (and structure), vegetation leaf on/off condition, canopy closure, and other environmental factors. Over marsh wetlands, the primary backscattering mechanism is volume backscattering, and with possible contributions from stalk-water double-bounce backscattering and/or specular scattering if the above-ground vegetation is short and the majority of the imaged surface is water [Fig. 1(b)].

After removing the topographic effect, the repeat-pass interferometric phase $(\phi)$ is approximately the incoherent summation of differences in surface backscattering phase $(\phi_{\rm s})$, volume backscattering phase $(\phi_{\rm v})$, and double-bounce phase $(\phi_{\rm d})$

$$\phi = (\phi_{\rm s2} - \phi_{\rm s1}) + (\phi_{\rm v2} - \phi_{\rm v1}) + (\phi_{\rm d2} - \phi_{\rm d1}) + n \qquad (1)$$

where $\phi_{\rm s1}$, $\phi_{\rm v1}$, and $\phi_{\rm d1}$ are the surface, volume, and double-bounce backscattering phase values, respectively, from the SAR image acquired at an earlier date; $\phi_{\rm s2}$, $\phi_{\rm v2}$, and $\phi_{\rm d2}$ are the corresponding phases from the SAR image acquired at a later date; and $n$ is the noise.

As the two SAR images are acquired at different times, the loss of interferometric coherence has to be evaluated. Loss of InSAR coherence is often referred to as decorrelation. Besides the thermal decorrelation, caused by the presence of uncorrelated noise sources in radar instruments, there are three primary sources of decorrelation over wetlands [24]–[26]: 1) geometric decorrelation resulting from imaging a target from different look angles; 2) volume decorrelation caused by volume backscattering effects; and 3) temporal decorrelation due to environmental changes over time.

Geometric decorrelation increases as the perpendicular baseline length increases, until a critical length is reached at which coherence is lost [27], [28]. For surface backscattering, most of the effect of baseline geometry on the measurement of interferometric coherence can be removed by the common spectral band filtering [29]. Because volume backscattering describes multiple scattering of the radar pulse that occurs within a distributed volume over wetlands, InSAR baseline geometry configuration can significantly affect volume decorrelation. As a result, volume decorrelation is most often coupled with geometric decorrelation and is a complex function of vegetation canopy structure that is difficult to simulate. Generally, the contribution of volume backscattering is controlled by the proportion of transmitted signal that penetrates the surface and the relative two-way attenuation from the surface to the volume element and back to the sensor [26]. Because both surface backscattering and volume backscattering consume and attenuate the transmitted radar signal, they determine the proportion of radar signal that is available to produce double-bounce backscattering. Surface backscattering and volume backscattering combine to lower InSAR coherence and reduce double-bounce backscattering that is utilized to measure water-level changes. Volume backscattering can be significantly affected by canopy closure; the volume decorrelation should be generally disproportional to canopy closure.

Temporal decorrelation describes any event that changes the physical orientation, composition, or scattering characteristics and spatial distribution of scatterers within an imaged volume. Over wetlands, these decorrelations are primarily caused by wind changing the leaf orientations, moisture condensation and rain changing the dielectric constant, flooding changing the dielectric and roughness of canopy background, and seasonal phenology, as well as anthropogenic activities such as cultivation and timber harvesting [26]. Temporal decorrelation is the net effect of changes in radar backscattering and therefore depends on the stability of the scatterers, the canopy penetration depth of the transmitted pulse, and the response to the changing conditions with respect to the wavelength.

It is clear that the geometric, volume, and temporal decorrelations are interleaved with each other and collectively affect InSAR coherence over wetlands. The combined decorrelations, which can be estimated using InSAR images (and are quantitatively assessed in Section V-C), determine the ability to detect water-level changes through the utilization of double-bounce backscattering signal.

When double-bounce backscattering dominates the returning radar signal, a repeat-pass InSAR image can be sufficiently coherent to allow the measurement of water-level changes from the interferometric phase values. The interferometric phase $(\phi)$ is related to the water-level change $(\Delta h)$ by

$$\Delta h = -\frac{\lambda \phi}{4\pi \cos\theta} + n \qquad (2)$$

where $\phi$ is the interferogram phase value, $\lambda$ is the SAR wavelength (5.66 cm for C-band ERS-1, ERS-2, and Radarsat-1), $\theta$ is the SAR incidence angle, and $n$ is the noise caused primarily by the aforementioned decorrelation effects.

## III. Study Site

Louisiana contains one of the largest expanses of coastal wetlands in the conterminous U.S. The coastal wetlands, built by the deltaic processes of the Mississippi River, contain an extraordinary diversity of habitats that range from narrow natural levee and beach ridges to expanses of forested swamps and marshes. Taken as a whole, the unique habitats of upland areas and the Gulf of Mexico, with their hydrological connections to each other, and migratory routes of birds, fish, and other species combine to place the coastal wetlands of Louisiana among the nation's most productive and important natural assets [30]. Our study area is over southeastern Louisiana (Fig. 2), and it includes the western part of New Orleans and the area between Baton Rouge and Lafayette.

The study area consists of primarily eight land cover types: urban, agriculture, bottomland forest, swamp forest, freshwater marsh, intermediate marsh, brackish marsh, and saline marsh. Agriculture and urban land covers are found in higher elevation areas and along the levee system. Bottomland forests exist in less frequently flooded lower elevation areas and along the lower perimeter of the levee system, while swamp forests are in the lowest elevation areas. Bottomland forests are dry during most of the year, and swamp forests are inundated. Both types

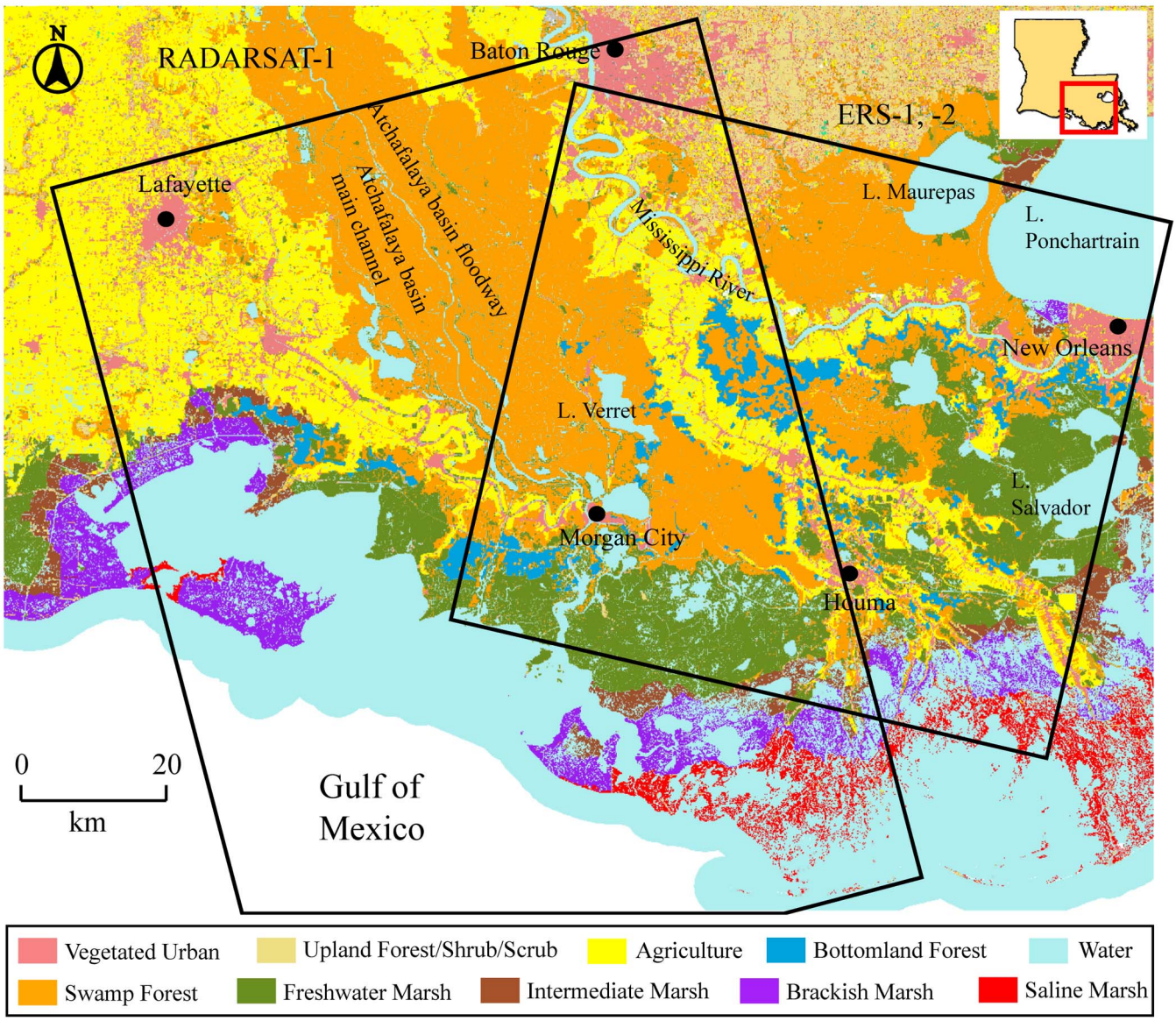


Fig. 2. Thematic map, modified from GAP and 1990 USGS-NWRC classification results, showing major land cover classes of the study area. Polygons represent extents of InSAR images shown in Fig. 4(a) for the ERS-1/ERS-2 and Radarsat-1 tracks, respectively.

of forests are composed largely of American elm, sweetgum, sugarberry, swamp red maple, and bald cypress [31].

Marshes, including saline, brackish, intermediate, and freshwater marshes, account for a major proportion of the biomass along the northeastern Gulf of Mexico coastal area. Freshwater marshes are composed largely of a floating marsh known locally as "flottant" and consist of vegetative mats of detritus, algae, and plant roots that support aquatic emergent plants such as maidencane, spikerush, and bulltongue (http://aquaplant.tamu.edu/database/index/visual_id_emergent_plants.htm). Intermediate marshes can be characterized by plant species common to freshwater marshes but with the saltier versions toward the sea and are largely composed of bulltongue and saltmeadow cordgrass [32]. Brackish marshes are largely composed of wire grass and three-square bulrush. Saline marshes are largely composed of smooth cordgrass, oyster grass, and saltgrass. The salinity increases from freshwater marsh, to intermediate marsh, to brackish marsh, and to saline marsh. Vegetation species decrease seaward because of the increase in salinity.

## IV. Data and Processing

### A. SAR Data

SAR data used in this paper consist of 33 scenes of ERS-1/ERS-2 images and 19 scenes of Radarsat-1 images. The ERS-1/ERS-2 scenes, spanning 1992–1998, are from a descending track with a radar incidence angle of about 20°–26°. The ERS-1/ERS-2 data are VV polarized. The Radarsat-1 scenes, spanning 2002–2004, are from an ascending track with a radar incidence angle of about 25°–31°. Unlike ERS-1/ERS-2, Radarsat-1 images are HH polarized. From these data, we produced 47 ERS-1/ERS-2 interferograms with perpendicular baselines less than 300 m [Fig. 3(a)] and 31 Radarsat-1

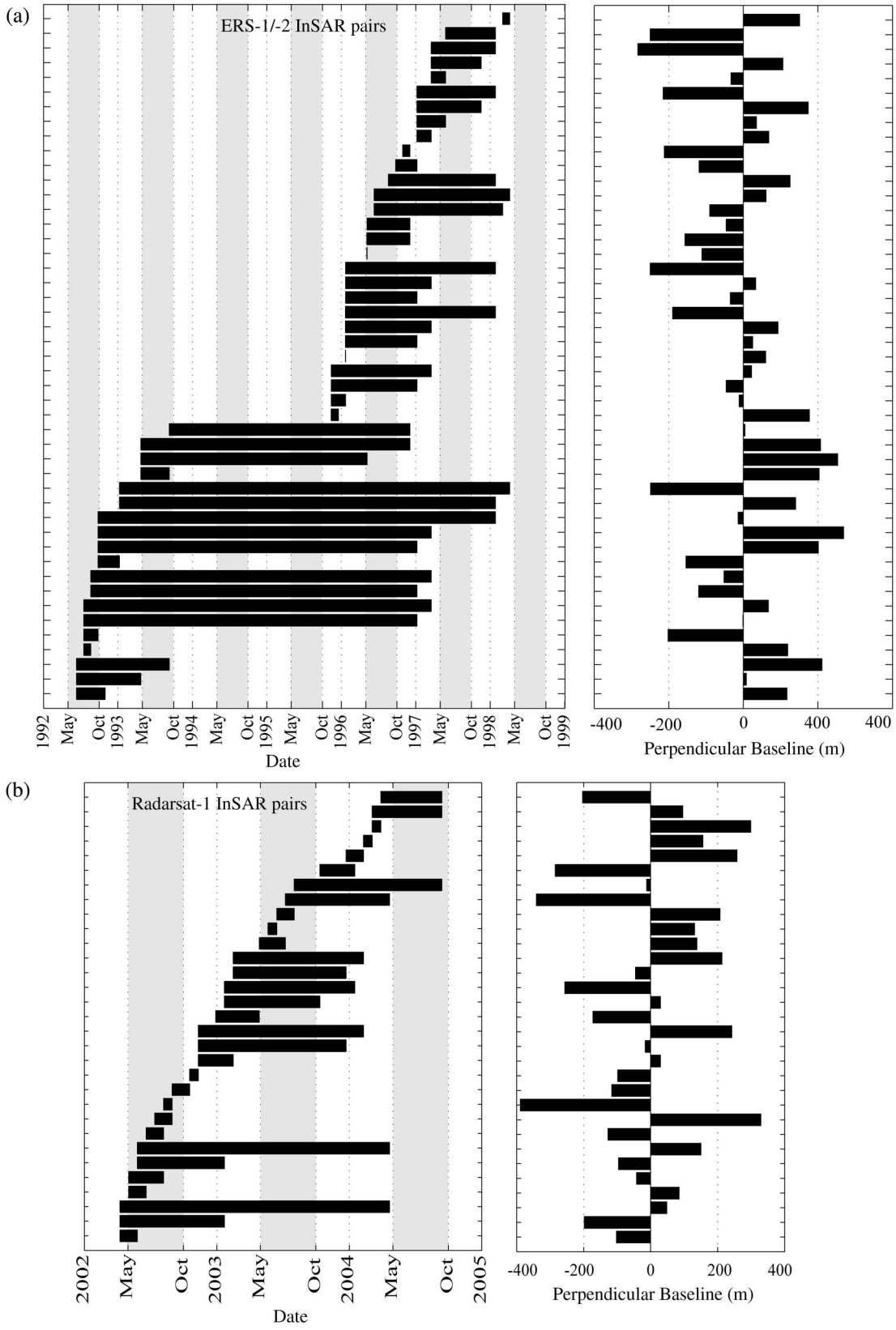


Fig. 3. InSAR image pair characteristics, including image acquisition times and their corresponding baselines for both ERS-1/ERS-2 and Radarsat-1 data used in this paper.

interferograms with perpendicular baselines less than 400 m [Fig. 3(b)]. The common spectral band filtering was applied to maximize interferometric coherence [29].

### *B. InSAR Processing*

For InSAR processing, the 30-m SRTM DEM is used. The study area is very flat, with height variations ranging from about

−9 to 23 m for 99.9% of the study area. For ERS-1/ERS-2 interferograms, we used the precision restituted orbital vectors from Delft University, The Netherlands [33]. The accuracy of the satellite position vectors provided in Radarsat-1 metadata is much poorer than the precision vectors for ERS-1 and ERS-2. Accordingly, the baselines of Radarsat-1 interferograms have to be refined. We utilized the fringe patterns over urban areas and agricultural fields (whenever interferometric coherence is maintained) to adjust the baseline so that the fringes over urban and agricultural areas are flattened. This can be done by perturbing the baseline values and calculating the average of interferometric coherence values over urban and agriculture areas through a computation-intensive search. The optimum baseline produces the highest coherence. Alternatively, one can model the fringes over nonwetland areas with a first-order or second-order polynomial function of range and azimuth coordinates and remove the best fit polynomial function from the whole interferogram. The latter is computationally efficient and often works.

Interferometric coherence was calculated using 15 by 15 pixels on ERS-1/ERS-2 interferograms that were generated with a multilook factor of 2 by 10 from the single-look-complex images and 11 by 11 pixels for Radarsat-1 interferograms with a multilook factor of 3 by 11. The large amount of pixels for coherence estimation can reduce the bias in coherence estimation [28], [34]. Therefore, although interferograms used to map water-level changes have spatial resolutions of about 40 and 53 m for ERS-1/ERS-2 and Radarsat-1 images, the coherence measurements were made over a spatial scale of about 600 m by 600 m. As significant fringes were observed over swamp forest areas, we "detrended" the fringes to calculate the coherence as follows. First, interferograms were filtered [35] and unwrapped with the minimum cost flow method [36]. The unwrapped interferometric phase images were then spatially smoothed with a boxcar filter of 7 by 7 pixels. Next, the unwrapped smoothed images were subtracted from the original interferometric phase images, and finally, the resultant phase images were used to calculate interferometric coherence values. This procedure significantly reduces artifacts caused by dense fringes on the coherence estimation.

## V. Results and Discussion

### A. Averaged Intensity Images

Fig. 4(a) shows the averaged ERS-1/ERS-2 SAR intensity image and the averaged Radarsat-1 intensity image. These averaged images were generated using all of the SAR intensity images for this paper. The primary focus of this paper is the region of overlap by the ERS-1/ERS-2 and Radarsat-1 images. Based on normalized difference vegetation index analysis by Kwoun and Lu [10], we define the months of May–September as the leaf-on season and the months of October–April as the leaf-off season.

Kwoun and Lu [10] conducted a detailed analysis of backscattering intensity variations over different land cover types. Radar backscattering values, calibrated with respect to the backscattering over urban land cover, are shown in Fig. 4(b). The radar backscattering from swamp forests exhibits the highest value among the vegetation classes in the study area, followed by bottomland forest, agriculture, saline marsh, freshwater marsh, intermediate marsh, and brackish marsh. The radar backscattering over swamp forests during leaf-off seasons is about 0.5 to 1.0 dB larger than during leaf-on seasons. The seasonal difference is more salient for HH-polarized Radarsat-1 data than VV-polarized ERS-1/ERS-2 imagery. The difference in radar backscattering between leaf-off and leaf-on seasons can barely reach about 0.2–0.3 dB for bottomland forests, where water is not present beneath the forests during most of the year. All of these suggest that double-bounce backscattering is the dominant backscattering mechanism for swamp forests for the study area, whereas volume backscattering is the primary scattering mechanism for bottomland forests [10].

Freshwater and intermediate marshes show very similar backscattering coefficients in both ERS and Radarsat-1. The saline marsh has the highest backscattering value whereas the brackish marsh has the lowest among the marsh classes [Fig. 4(b)]. The saline marsh generally has a significantly higher backscattering than other marsh classes and is similar to those from agriculture and bottomland forest. Based on the seasonal change in backscattering coefficients for all marsh classes, Kwoun and Lu [10] suggested the following: 1) the primary backscattering mechanism for saline marsh is double-bounce backscattering; 2) volume backscattering dominates C-band radar interactions with freshwater and intermediate marshes; and 3) brackish marsh is characterized primarily by specular scattering. Finally, Radarsat-1 backscattering coefficients offer better separability among different wetland land cover types than ERS data, suggesting that C-band HH polarization is more sensitive to structural differences than C-band VV polarization over the study area [10]. Based on our results, we infer that a similar multitemporal multipolarization backscattering analysis technique may be applicable for vegetation classification over other regions of the world. Obviously, the multitemporal analysis of fully polarimetric SAR will significantly improve the separability among different types of vegetation [38].

### B. Observed InSAR Images

Fig. 5 shows a few examples of ERS-1/ERS-2 InSAR images. Fig. 5(a)–(d) shows the interferograms acquired during leaf-off seasons, with time separations of 1 day [Fig. 5(a)], 35 days [Fig. 5(b)], 70 days [Fig. 5(c)], and 5 years [Fig. 5(d)]. The one-day interferogram [Fig. 5(a)] during the leaf-off season is coherent for almost every land cover class except open water. In the one-day interferogram, a few localized areas exhibit interferometric phase changes which are most likely a result of water-level changes over the swamp forests. The large-scale phase changes over the southeastern part of the interferogram are likely caused by atmospheric delay anomalies. Most of the land cover classes (Fig. 2), except open water, bottomland forests, and some of the freshwater and intermediate marshes, are coherent in the 35-day interferogram [Figs. 2 and 5(b)]. The interferogram clearly shows the water-level changes over both swamp forests and marshes [Fig. 5(b)]. The overall coherence

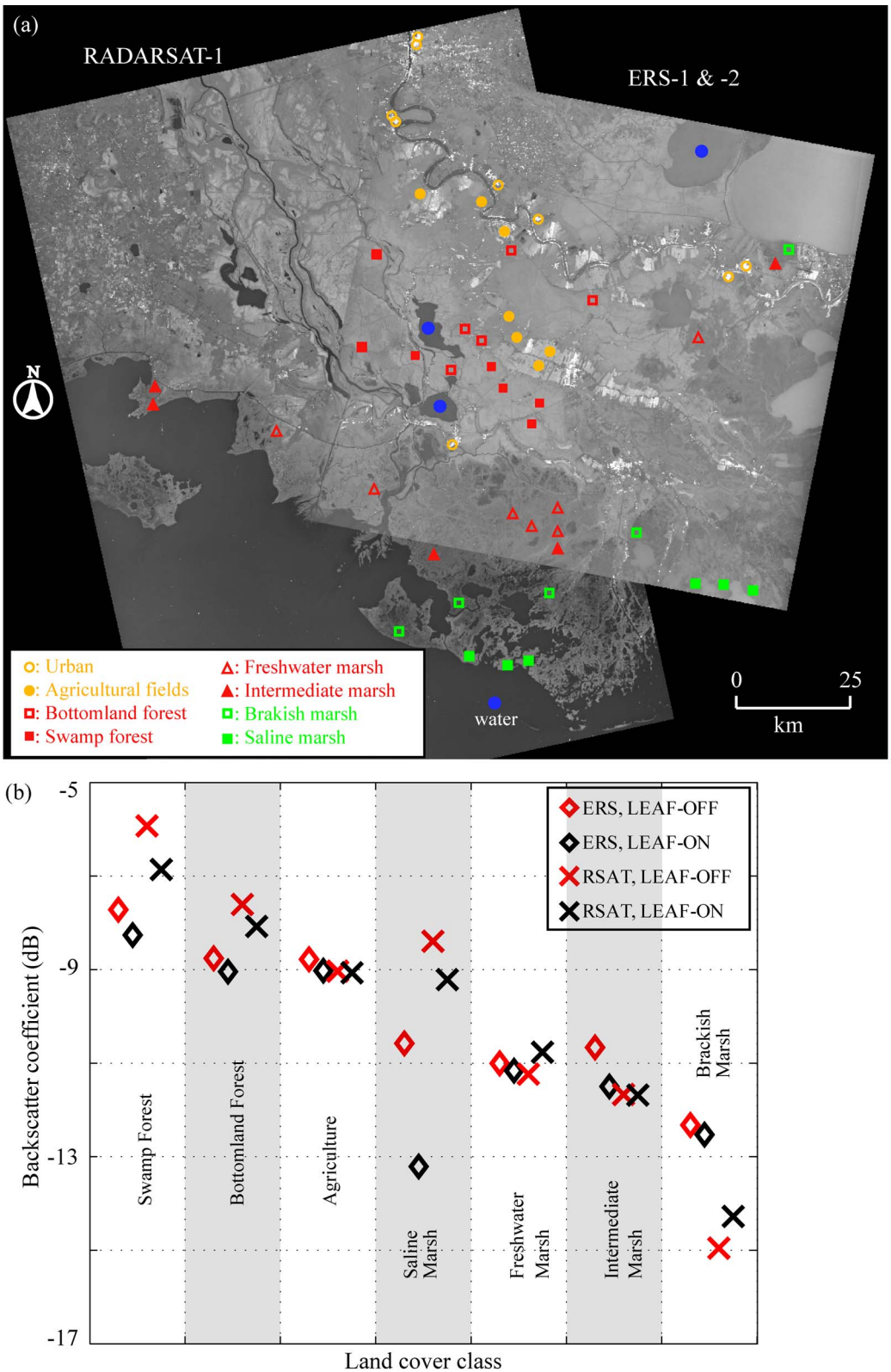


Fig. 4. (a) Averaged ERS-1/ERS-2 and Radarsat-1 intensity images showing locations where quantitative coherence analyses were conducted. (b) Averaged radar backscattering coefficients (relative to urban backscattering returns) for seven major land cover classes during both leaf-on and leaf-off seasons.

for the 70-day interferogram [Fig. 5(c)] is generally lower than the 35-day interferogram [Fig. 5(b)]. In 70 days [Fig. 5(c)], bottomland forests, freshwater marshes, and intermediate marshes completely lose coherence, although some saline and brackish marshes can maintain coherence. Over five years, some swamp forests and urban areas can maintain coherence [Figs. 2 and 5(d)]. Coherence can be maintained for swamp forests for over five years, which strongly suggests that the dominant scattering mechanism is double-bounce backscattering, supporting the conclusion by Lu *et al.* [16].

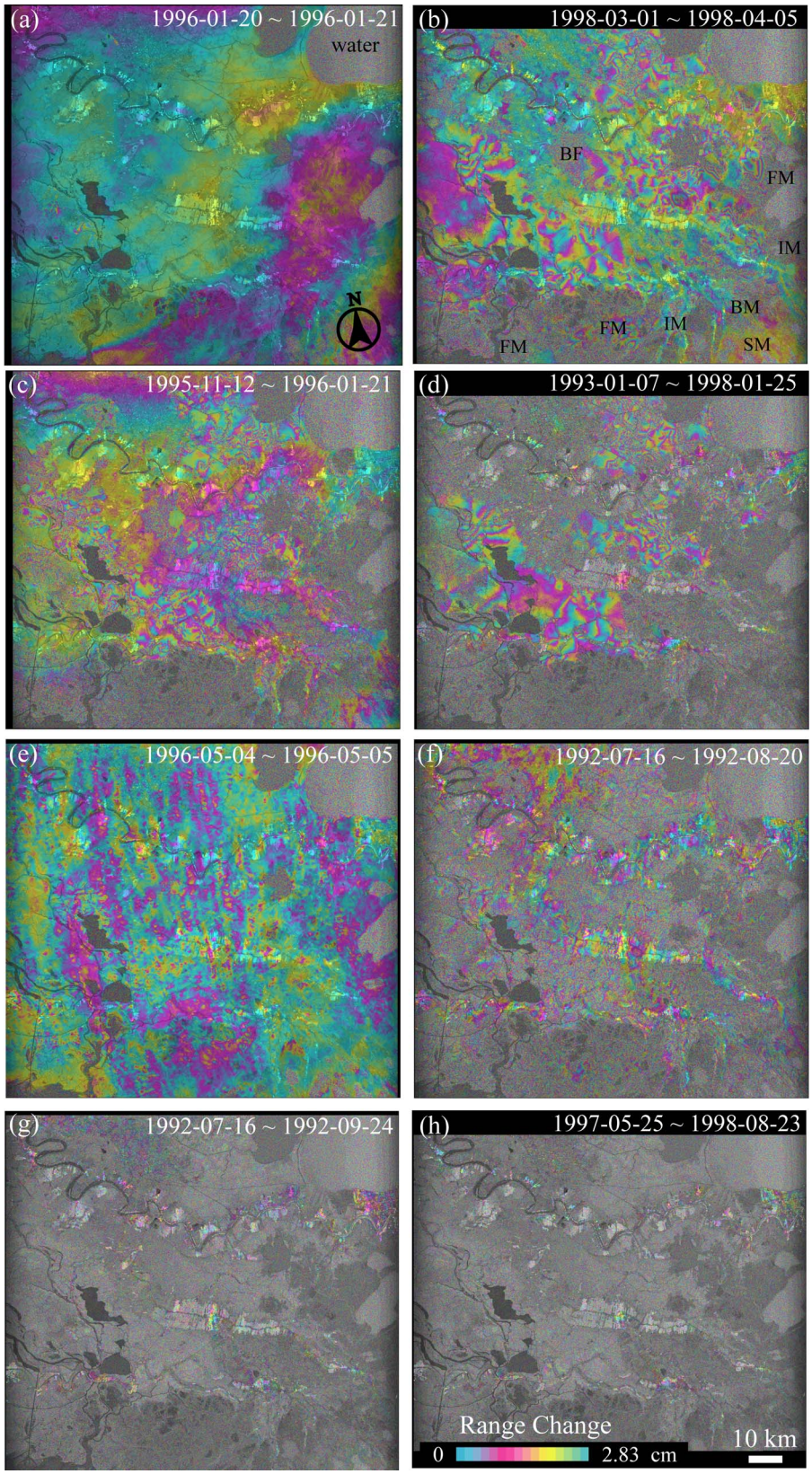


Fig. 5. Examples of ERS-1/ERS-2 InSAR images with different time separations during (a)–(d) leaf-off and (e)–(h) leaf-on seasons. BF—bottomland forest; FM—freshwater marsh; IM—intermediate marsh; BM—brackish marsh; SM—saline marsh.

Fig. 5(e)–(h) shows interferograms from ERS-1/ERS-2 SAR images acquired during leaf-on seasons, with time separation of 1 day [Fig. 5(e)], 35 days [Fig. 5(f)], 70 days [Fig. 5(g)], and 1 year [Fig. 1(h)]. Compared with the corresponding interferograms acquired during leaf-off seasons with similar time intervals [Fig. 5(a)–(d)], the leaf-on interferograms generally exhibit

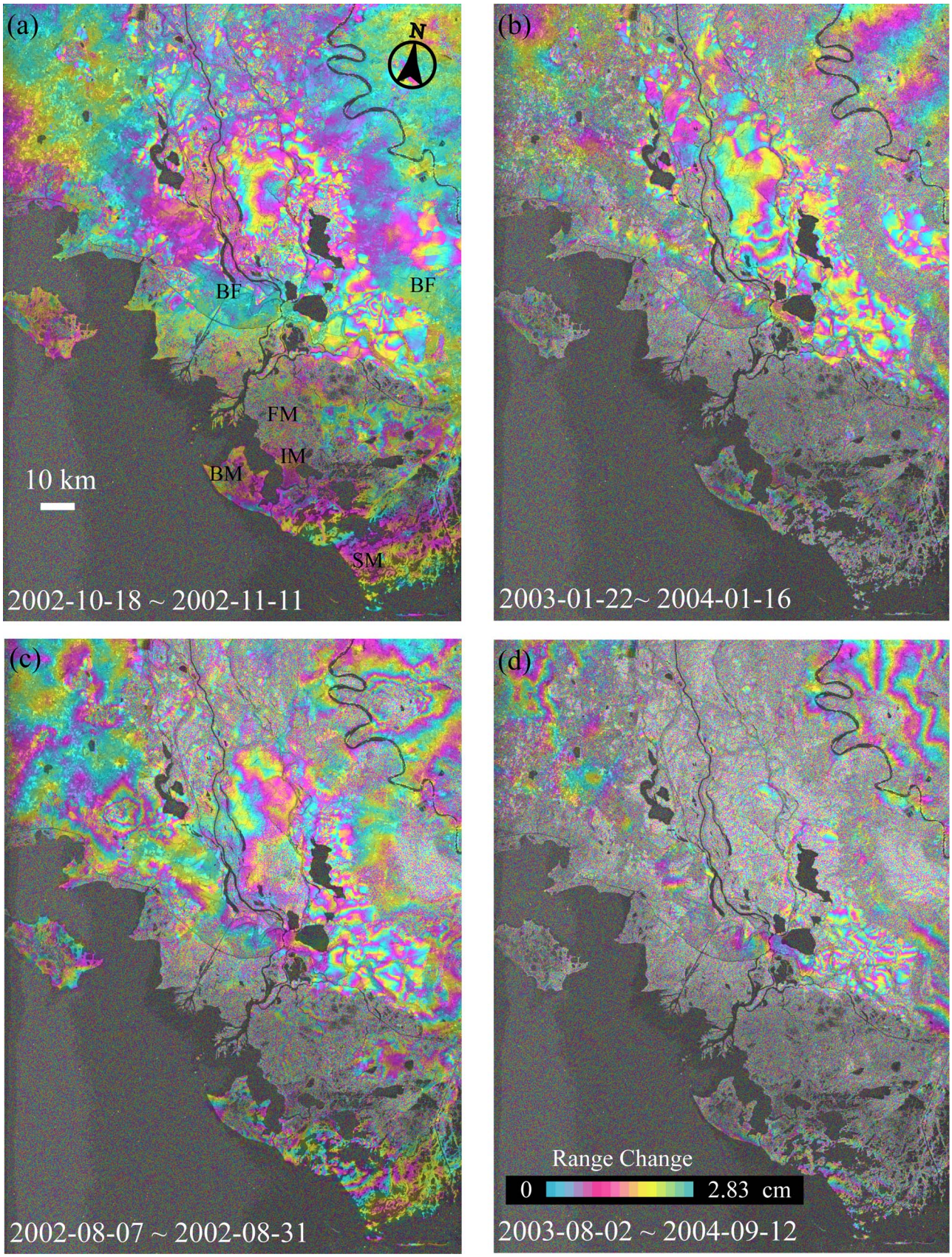


Fig. 6. Examples of Radarsat-1 InSAR images with different time separations during (a)–(b) leaf-off and (c)–(d) leaf-on seasons. BF—bottomland forest; FM—freshwater marsh; IM—intermediate marsh; BM—brackish marsh; SM—saline marsh.

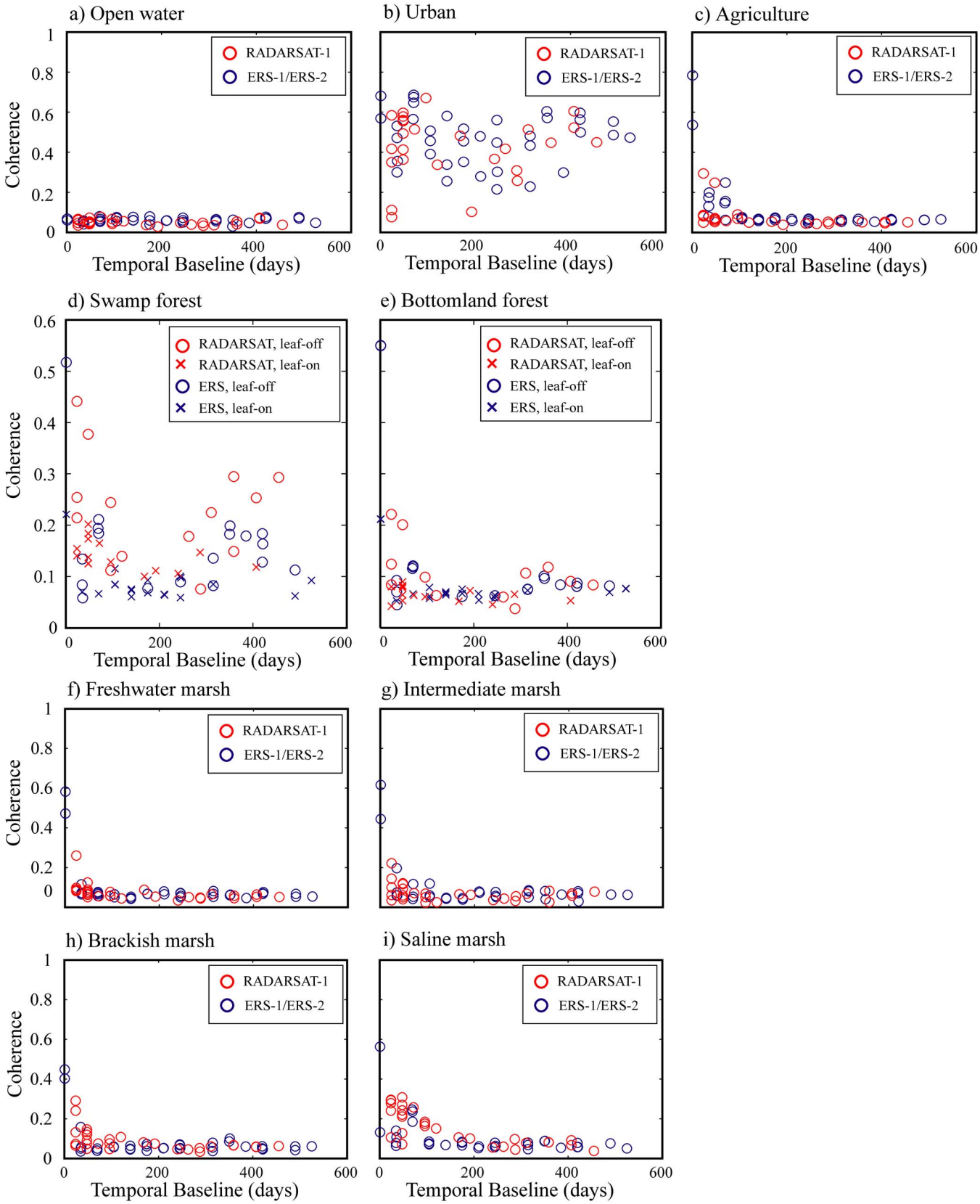


Fig. 7. InSAR coherence as a function of time separation for major land cover classes as follows. (a) Open water, (b) urban, (c) agriculture, (d) swamp forest, (e) bottomland forest, (f) freshwater marsh, (g) intermediate marsh, (h) brackish marsh, and (i) saline marsh for both ERS-1/ERS-2 and Radarsat-1 interferograms acquired during leaf-off and leaf-on seasons. The scale for Fig.7(d) and (e) is different from the others in order to illustrate that seasonality is one of the factors controlling coherence for forests.

much lower coherence. All of the land cover classes (Fig. 2) maintain coherence in one day [Fig. 5(e)]. For most of the land cover classes, except urban, agriculture, and portions of swamp forests, interferometric coherence cannot be maintained after 35 days [Fig. 5(f)–(h)]. With a time interval of 70 days, only urban and some agriculture fields have coherence [Fig. 5(g)]. Over one year, only urban areas maintain some degree of coherence [Fig. 5(h)]. We speculate that the overall reduction in interferometric coherence for swamp forests during leaf-on seasons is because the dominant backscattering mechanism is not double-bounce backscattering but the combination of surface and volume backscattering.

Fig. 6(a) and (b) shows two Radarsat-1 interferograms acquired during leaf-off seasons. The interferometric coherence for the 24-day HH-polarization Radarsat-1 interferogram [Fig. 6(a)] is generally higher than the 35-day VV-polarization ERS-1/ERS-2 interferogram [Fig. 5(b)]. In 24 days, only water and some freshwater marshes do not have good coherence [Fig. 6(a)]. We notice that bottomland forests (Fig. 2) can maintain good coherence for 24 days. From Fig. 6(b), it is obvious that some swamp forests and urban areas maintain coherence for more than one year.

Fig. 6(c) and (d) shows Radarsat-1 interferograms during leaf-on seasons. Again, the 24-day HH-polarization Radarsat-1 interferogram maintains higher coherence than the 35-day VV-polarization ERS-1/ERS-2 images [Fig. 5(f)] for most land cover types. It is surprising that the one-year Radarsat-1 interferogram during leaf-on seasons [Fig. 6(d)] can maintain relatively high coherence over parts of swamp forests and saline marshes. In general, although Radarsat-1 coherence is reduced during leaf-on seasons, the reduction in the coherence for Radarsat-1 is much less than that for ERS-1/ERS-2. Over a similar time interval, HH-polarized Radarsat-1 interferograms have higher coherence than VV-polarized ERS-1/ERS-2 interferograms.

During a very dry season or a period of extremely low water, even swamp forests can be exposed to dry ground. Among the interferograms in our study area, patches of swamp forests can lose coherence. We speculate that this is probably because there was no water beneath the swamp forest at the image acquisition times. Therefore, the double-bounce backscattering mechanism is diminished, and the dominant backscattering mechanism for "dried" swamp forests is the same as that for bottomland forests. Alternatively, bottomland forests can be flooded occasionally. The presence of water on bottomland forests produces double-bounce backscattering and, accordingly, makes the radar backscattering return from a bottomland forest similar to that from a swamp forest.

### C. Interferometric Coherence Analysis

As it is only possible to detect water-level changes beneath wetlands from coherent InSAR images, we quantitatively assess variations of interferometric coherence over the study area. Fig. 7 shows the InSAR coherence measurements for different land cover types. For each of the land cover classes, we calculated coherence for several locations, selected as representatives of each land cover class. The size of the polygon is about 600 m by 600 m for both ERS-1/ERS-2 and Radarsat-1 images. We first determined thresholds of complete decorrelation for ERS-1/ERS-2 and Radarsat-1 interferograms by calculating interferometric coherence values over open water with the same polygon size (600 m by 600 m). In Fig. 7, the coherence measurements from both leaf-on and leaf-off seasons are combined for all classes except for swamp and bottomland forests because the seasonality is a critical factor that controls the interferometric coherence of forests. The dependence of the interferometric coherence on spatial baseline was also explored. For the interferograms used in this paper, we found no dependence between the interferometric coherence and the perpendicular baseline. This is because more than 70% of the interferograms have perpendicular baselines of less than 200 m and that the common spectral band filtering [29], [39] was applied during the interferogram generation.

Fig. 7(a) shows coherence over open water. Because open water completely loses coherence for repeat-pass interferometric observations, its coherence value can be regarded as the threshold of complete decorrelation (loss of coherence). The coherence values for both ERS-1/ERS-2 and Radarsat-1 InSAR images are about $0.06 \pm 0.013$. In this paper, coherence values that are smaller than 0.1 will be regarded as complete decorrelation.

We chose several sites [Fig. 4(a)] to show coherence over urban areas: Six of them are located along the Mississippi River and one in Mogan City which is more vegetated than the other urban sites. Fig. 7(b) shows interferometric coherence measurements over urban sites from both ERS-1/ERS-2 and Radarsat-1 interferograms. Overall coherence measurements from both ERS-1/ERS-2 and Radarsat-1 images are similar, and they are higher than any other land cover class. However, they vary in the range of about 0.2–0.7. The variations are most likely a result of decorrelation caused by vegetation over the urban areas. Vegetation in urban areas can alter radar backscattering coefficients by more than 8 dB [10]. Urban areas with lower radar backscattering intensities tend to be associated with lower interferometric coherence values, suggesting that the vegetation in urban areas causes lower radar backscattering coefficients as well as reduced coherence measurements.

Fig. 7(c) shows coherence measurements over agriculture fields. Because of frequent farming activities with multiple harvesting, a complete decorrelation is reached in about 100 days. This implies that the vegetation condition in these fields changes completely in about 100 days.

Fig. 7(d) shows interferometric coherence measurements from swamp forests. Comparing the coherence measurements from ERS-1/ERS-2 and Radarsat-1 images, we can make the following inferences. First, coherence is higher during leaf-off seasons than during leaf-on seasons for both ERS-1/ERS-2 and Radarsat-1 images. Second, the coherence from HH-polarization Radarsat-1 images is generally higher than that from VV-polarization ERS-1/ERS-2 images. Third, the coherence from both Radarsat-1 images and ERS-1/ERS-2 images during leaf-off season can last over two years [Fig. 7(d)]. If the scattering elements came primarily from the top of the forest canopy, it is unlikely that the SAR signal would be coherent over a period of about one month or longer [24], [25]

because leaves and small branches comprising the forest canopy change due to weather conditions. Based on interferometric coherence [Fig. 7(d)] and backscattering coefficient values [Fig. 4(b)] during leaf-off and leaf-on seasons, we conclude that the dominant radar backscattering mechanism over swamp forests during the leaf-off seasons is double-bounce backscattering. As a result, Radarsat-1 and ERS-1/ERS-2 images during leaf-off seasons are capable of imaging water-level changes over swamp forests. During leaf-on seasons, HH-polarization Radarsat-1 images can maintain coherence for a few months, reaching up to about 0.2. If HH-polarized C-band radar images were acquired for shorter time intervals during leaf-on seasons, they would also be used for measuring water-level changes.

Fig. 7(e) shows coherence measurements for bottomland forests. We can see that the coherence is higher during leaf-off seasons than leaf-on seasons. The HH-polarization Radarsat-1 images tend to have higher coherence than the VV-polarized ERS-1/ERS-2 images for short temporal separations (less than about two months). The coherence from both ERS-1/ERS-2 and Radarsat-1 images decreases exponentially with time. ERS-1/ERS-2 images become decorrelated in about one month while Radarsat-1 can maintain coherence up to about two months [Fig. 7(e)]. The difference in radar backscattering coefficient and interferometric coherence between swamp and bottomland forests is primarily caused by the double-bounce backscattering over swamp forests. The water beneath the trees enhances the double-bounce backscattering for swamp forests, producing higher InSAR coherence as well as stronger backscattering coefficient values. For bottomland forests, forest understory attenuates radar signal returns and the double-bounce backscattering is retarded, resulting in relatively lower coherence as well as smaller backscattering values than that of swamp forests. Other factors also affect the difference in backscattering between swamp and bottomland forests over the study area. The two forest types are structurally different. The bottomland forests have broad leaves and deterrent structures where the lateral branches form wide and bell-shaped crowns, whereas swamp forests tend to have needle leaves and excurrent structures, producing somewhat cone-shaped crowns. In addition, swamp forests display a fairly to highly nonuniform canopy, with frequent gaps of a few meters and large canopy height variations. Compared to the swamp forests, bottomland forests tend to exhibit a wide range of dense forest types with diverse understories. From the perspective of scatterer roughness within a SAR resolution cell, forests with large height variations tend to exhibit stronger backscattering than uniform height forests, and forests with gaps tend to show stronger backscattering signal than that of dense forests (G. Sun, personal communication, 2007). Therefore, swamp forests have both stronger backscattering returns and higher coherence values than the bottomland forests over the study site.

The above coherence analysis suggests that SAR images, preferably HH-polarized, can maintain good coherence over both swamp and bottomland forests for about one month. Accordingly, shorter temporal separations (a few days) will significantly improve the InSAR coherence for the detection of water-level changes.

Fig. 7(f)–(i) shows coherence measurements over marshes. Coherence measurements are generally higher from HH-polarized Radarsat-1 images than from VV-polarized ERS-1/ERS-2 images; ERS-1/ERS-2 can barely maintain coherence for about one month, whereas Radarsat-1 maintains coherence up to about three months. The coherence values for intermediate, freshwater, and brackish marshes are similar, and they are lower than those for saline marshes. Overall, saline marsh has the highest coherence [Fig. 7(i)] as well as the highest backscattering value [Fig. 4(b)] among marsh classes, suggesting that saline marshes tend to develop more dominant vertical structure than other marshes to allow double-bounce backscattering of C-band radar waves. Over intermediate and freshwater marshes, the surface and volume backscattering mechanisms are the primary backscattering mechanism, and the backscattering return depends on the amount of emerged biomass [40]. For brackish marshes, specular scattering can be dominant during some portion of the year. As marshes can only maintain coherence in less than 24 days, repeat-pass SAR images should be acquired over short time intervals (a few days) for the purpose of robust detection of water-level changes.

### *D. InSAR-Derived Water-Level Changes*

Fig. 8 shows several examples of coherent ERS-1/ERS-2 and Radarsat-1 interferograms with short temporal separations, where interferometric phase values were used to study changes in the water level of swamp forests. Each interferogram shows the relative changes in water level between dates when the two images were acquired. Each fringe represents a range (distance from the satellite to ground) change of 2.83 cm, or about 3.07-cm water-level change for ERS-1/ERS-2 InSAR images and 3.20 cm for Radarsat-1 images. From the interferograms in Fig. 8, we can make the following inferences.

1) The changes in water level are dynamic. For example, Fig. 8(i) shows the change in water level reaching as much as 36 cm over a distance of about 37 km. The direction and the density of fringes within the Atchafalaya Basin Floodway (ABF) are spatially varying. Such changes in water level reflect local differences in topographic constrictions and vegetation resistance to the surface flow. Flooding throughout this area is primarily by sheet flow after the rivers and bayous leave their banks. Under ideal circumstances, water should flow placidly and smoothly over a symmetrically smooth surface devoid of obstructions. Thus, the sheet flow should not be symmetric throughout the study area, i.e., it should not be a smooth even surface of constant elevation from one edge of the swamp to the other. Instead, there should be bulges and depressions in the water surface as a result of topographic constrictions and vegetation resistance in sheet flow.
2) The changes in water level are not homogeneous. First, the observed fringes exhibit evidence of control by structures such as levees, canals, bayous, and roads, resulting in abrupt changes in interferometric phase value. The heterogeneity in water-level change is due primarily to these man-made structures and artificial boundaries.

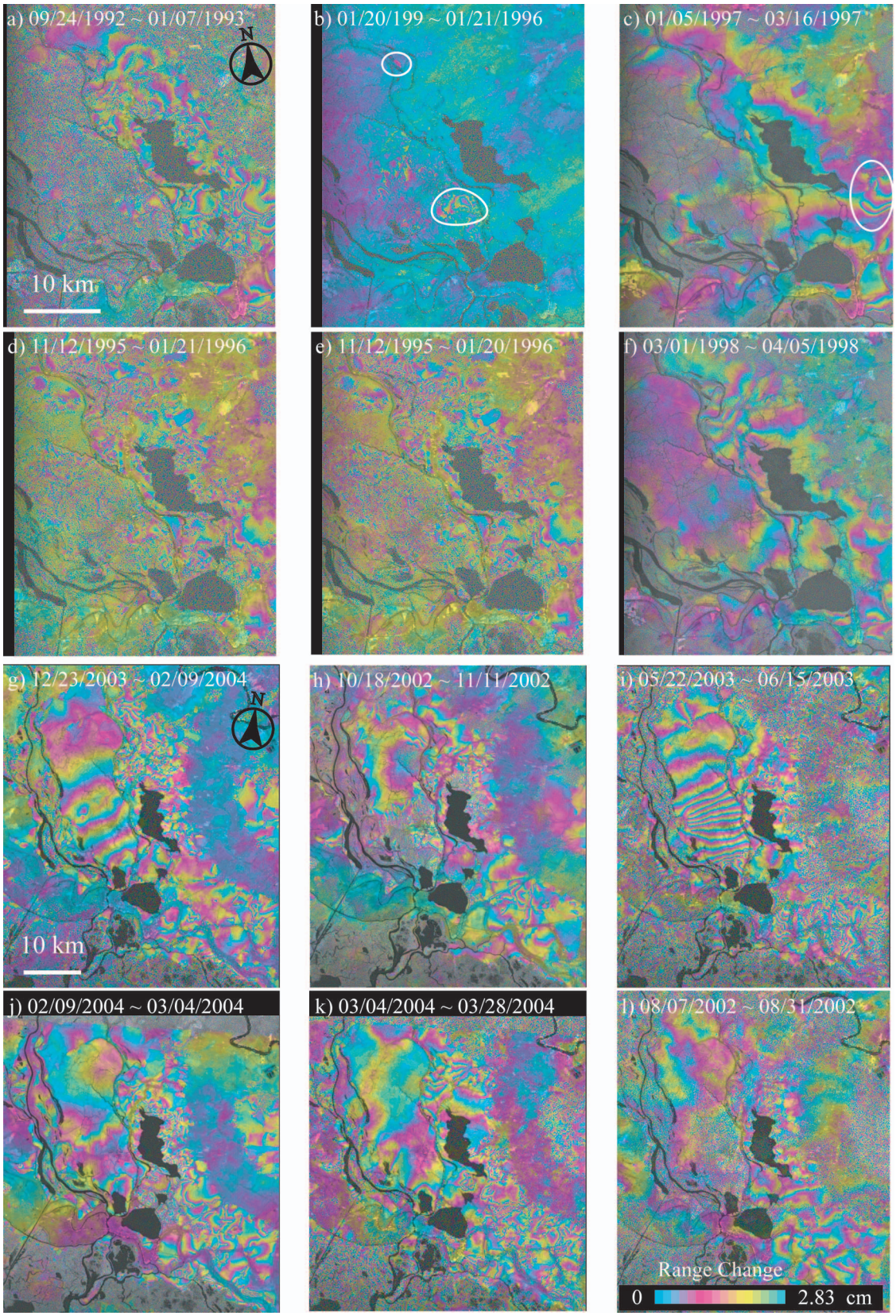


Fig. 8. (a)–(f) ERS-1/ERS-2 and (g)–(l) Radarsat-1 Interferograms with good coherence and short temporal separations, used to illustrate the heterogeneity of water-level changes.

Second, within the ABF, the observed interferometric fringes are bent [e.g., Fig. 8(h)–(k)]. This suggests that local variations in vegetation cover resist water flow variably. Heterogeneous water-level changes such as these make it impossible to accurately characterize water storage based on measurements from a few sparsely

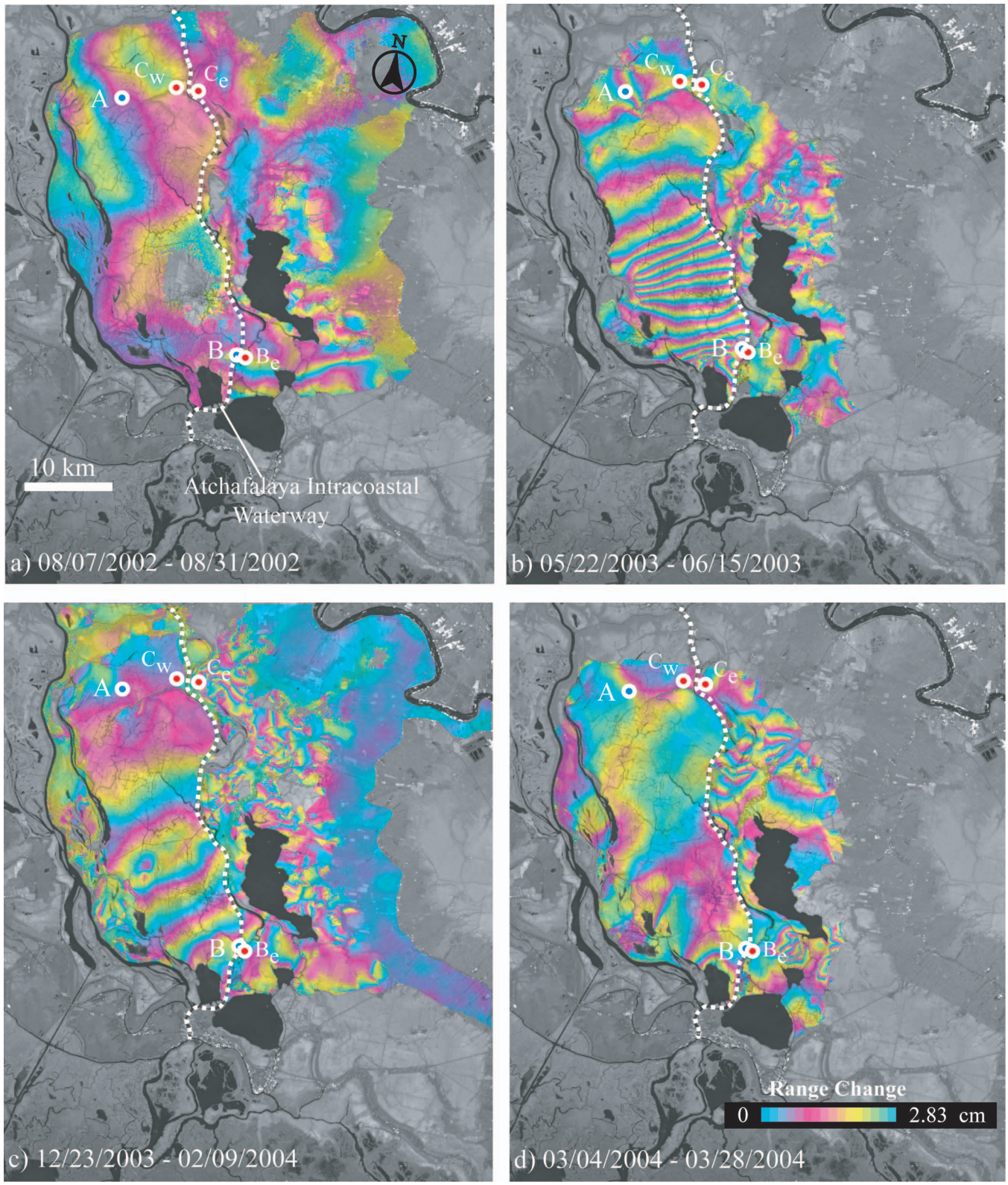


Fig. 9. Unwrapped Radarsat-1 images used to quantify water-level changes. InSAR-derived water-level changes at the selected locations are compared with gauge readings (see Table I for details).

distributed gauge measurements. This demonstrates the unique capability of InSAR to map water-level changes in unprecedented spatial detail. This is the most promising aspect of mapping water-level changes with InSAR.

3) Interferograms in Fig. 8 reveal both localized and relatively large-scale changes in water level. On the one hand, localized changes in water flow can be found in the 24-h interferogram (outlined in white in [Fig. 8(b)] and

TABLE I
COMPARISON OF WATER-LEVEL-CHANGE MEASUREMENTS BETWEEN INSAR AND GAUGE STATIONS. A AND B ARE TWO GAUGE STATIONS WITHIN THE SWAMP FOREST WEST OF AICWW (FIG. 9). C IS A POINT OVER THE AICWW WHERE INSAR IMAGES ARE NOT COHERENT. $C_w$ AND $C_e$, TWO INTERFEROMETRICALLY COHERENT POINTS NEAR C, ARE LOCATED OVER THE SWAMP FOREST WEST AND EAST OF THE AICWW, RESPECTIVELY. $B_e$ IS A POINT ADJACENT TO B. BOTH $C_w$ AND B ARE WITHIN THE SWAMP FOREST WEST OF THE AICWW, AND $C_e$ AND $B_e$ ARE OVER THE SWAMP FOREST EAST OF THE AICWW (FIG. 9)

| Date | InSAR measurements | Gauge readings | InSAR measurements | |
|---|---|---|---|---|
| | A - B (cm) | A - B (cm) | $C_w$ - B (cm) | $C_e$ - $B_e$ (cm) |
| 08/07/2002-08/31/2002 | -0.01 | -0.60 | -1.38 | -2.01 |
| 05/22/2003-06/15/2003 | 36.10 | N/A | 31.34 | 6.61 |
| 12/23/2003-02/09/2004 | 13.63 | 11.44 | 13.99 | 1.34 |
| 03/04/2004-03/28/2004 | 3.99 | 5.19 | 5.68 | -0.96 |

the 70-day interferogram during January–March 1997 (outlined in white in [Fig. 8(c)]. On the other hand, relatively large-scale changes in water level can be observed across much of the water basin [e.g., Fig. 8(g) and (i)].

Because the interferometric fringes are dissected by rivers, canals, levees, roads, and other structures, interferometric phase measurements can be disconnected at these boundaries. In other words, interferometric phase measurements at two nearby pixels separated by these boundaries are discontinuous. This adds enormous complexity to understanding water-level changes inferred from InSAR measurements. Furthermore, calculating water-level changes along two different paths that are separated by these boundaries can lead to different estimates of water-level changes. We chose four Radarsat-1 interferograms (Fig. 9) to illustrate this. We first unwrapped the interferograms piecewise using the branch-cut method [37]. In particular, the regions to the west and east of the Atchafalaya Intracoastal Waterway (AICWW) were unwrapped separately. The interferometric coherence along the AICWW is often lost. To investigate water-level changes quantitatively, we selected several locations, including two gauge locations (Cross Bayou station at A and Sorrel station at B). Both A and B lie within the swamp forests west of AICWW, and we can extract the phase measurements at the exact locations of A and B. To the east of B and across the AICWW, we choose a location $B_e$ (Fig. 9) over the swamp forest east of the AICWW where InSAR coherence is maintained. Lastly, we selected a location C over the upstream of AICWW (Fig. 9). Because the interferometric coherence is not maintained at C, we chose two locations immediately adjacent to C: One is over the swamp forest to the west of AICWW ($C_w$ in Fig. 9), and the other over the swamp forest to the east of AICWW ($C_e$ in Fig. 9). Interferometric coherence is maintained at $C_w$ and $C_e$, and consequently, we can measure phases at these two points.

We first compared the water-level changes measured by InSAR and recorded at gauges at A and B to validate the reliability of the InSAR-based measurements of water-level changes. The daily gauge data represent water level at 8 A.M. local time (C. Swarzenski, personal communication, 2005), while Radarsat-1 images were acquired at 6 P.M. local time. Therefore, to match satellite image acquisition time, we interpolated gauge readings from the image acquisition date and the following date. Table I summarizes the results of water-level changes from gauges and from the interferograms in Fig. 9. The InSAR-derived water-level changes at A and B are in good agreement with gauge readings and within about 2-cm overall discrepancy. This indicates that water-level-change measurement by InSAR can be as good as that by gauges. As such, we can infer that the water-level changes detected by InSAR in areas not covered by gauges may be trusted. If this is the case, then the InSAR technique provides a unique way to map dynamic and heterogeneous water-level changes at accuracy comparable to gauges and at a spatial resolution unattainable by gauges. The gauge data at Cross Bayou (A in Fig. 9) on May 22, 2003, do not exist so we could not confirm water-level changes of about 36 cm detected by InSAR [Fig. 9(b)]. If we extend the perceived correspondence of about 2 cm between InSAR and gauge measurements, we can estimate the gauge reading at A to be about 437 cm around 6 P.M. local time on May 22, 2003. This demonstrates the utility of InSAR-based water-level-change measurement to augment the missing gauge data.

We next compare and quantitatively examine the water-level changes measured along two different paths ($C_w - B$ and $C_e - B_e$) within two swamp forest bodies separated by the AICWW. Please note locations $C_w$ and B are within the swamp forest west of AICWW and locations $C_e$ and $B_e$ are within the swamp forest east of AICWW. Integrating interferometric phase measurements along the western path $(C_w - B)$ and the eastern path $(C_e - B_e)$ gives water-level changes ranging from about $-1$ cm to 31 cm (Table I). For example, the water-level change between $C_w$ and B is about 31.34 cm whereas it is about 6.61 cm between $C_e$ and $B_e$ for the May 22, 2003, and June 15, 2003, InSAR image [Fig. 9(b)]. We interpret this to be a result of structures that obstruct smooth and rapid water flow, primarily within the swamp forests west of AICWW. The change in fringe pattern across the AICWW suggests that parts of the AICWW also act as barriers to continuous water flow in this area. Water-level changes in swamp forests over the study area are heterogeneous and disconnected by structures and other barriers, and therefore cannot be represented adequately by sparsely distributed gauge stations. This finding can be useful for hydrologists to enhance surface water flow models by correctly defining the spatial extent of homogeneous continuum

and for emergency planners to simulate the dynamics of flood water in the region with enhanced accuracy.

## VI. Discussions and Conclusion

The ability to map water-level changes at high spatial resolution with InSAR makes it an attractive tool for studying many hydrological processes. To adequately characterize the heterogeneous water-level changes over a complex wetland system requires many ground-based measurements, which can be cost-prohibitive. In this paper, we have demonstrated that C-band InSAR images can map water-level changes of coastal wetlands of Louisiana. Particularly, HH-polarized C-band InSAR can maintain good coherence for mapping water-level changes over coastal wetlands if the SAR images are acquired in a few days. Because L-band InSAR images generally maintain much higher coherence than C-band InSAR, L-band InSAR can map water-level changes over denser forests such as the Amazon rain forests [13], [14]. Combining C-band and L-band InSAR images can significantly improve temporal sampling of water-level measurements.

However, there are several shortfalls regarding water-level measurements from InSAR images. First, InSAR requires the presence of emergent vegetation [13]–[16] or structures in water [41] to allow radar signals to be scattered back to the antenna in order to measure water-level changes. Over open-water bodies, InSAR is useless for detecting water-level changes.

Second, a repeat-pass InSAR image measures the relative spatial gradient of water-level changes between two times. In other words, from interferometric phase measurements alone, we cannot derive the absolute volumetric change of water storage within a wetland without additional constraints. In an extreme case, we can assume that the water level over a wetland moves up or down by a constant height. The volumetric change of water over the wetland can be calculated by the area extent of the wetland and the constant height of water-level change. However, an InSAR image can only exhibit a constant phase value, which suggests no water-level changes over the wetland. Therefore, to estimate the volumetric change of water storage, the absolute water-level change at a single location within a wetland body is required. The situation can become even more complicated if the wetland system consists of many wetland bodies which are bounded by structures such as levees, canals, and other barriers, all of which can disconnect the InSAR phase values. In this case, it may be impossible to estimate volumetric storage change of the whole wetland system without knowing the absolute water-level change at a single location within each wetland body.

Another limitation of repeat-pass InSAR is that the atmospheric delay signal obscures radar signal associated with surface elevation changes. As an approximation, we can utilize the characteristics of both observed fringes and SAR backscattering returns to roughly infer whether certain fringes over wetlands are dominantly due to actual water-level changes or contaminated by atmospheric artifacts. The fringes due to water-level changes exhibit evidence of control by structures such as levees, canals, bayous, and roads (which are clearly observable from the SAR intensity image), resulting in abrupt changes in interferometric phase value (Figs. 8 and 9). If a certain fringe pattern extends across such structure features [e.g., the large-scale fringe pattern over the lower right quadrant of Fig. 5(a) or the upper right quadrant of Fig. 8(c)], we interpreted that the fringe was probably affected by atmospheric delay anomaly. However, the small-scale dense fringes inside the white ellipse in Fig. 8(c) are constrained by structures and water barriers identifiable from the SAR backscattering intensity image; we interpreted that these fringes were probably dominant from water-level changes. Atmospheric delay anomalies can reduce the accuracy of interferometrically derived water-level measurements from several millimeters in ideal conditions to several centimeters under coastal regions such as our study area. Over the wetland areas, we were unable to estimate the range of atmospheric delay anomalies. By inspecting a stack of ERS-1/ERS-2 images over the city of New Orleans, it was found that about 40%–50% of interferograms were affected by atmospheric delay anomalies (Kwoun and Lu, unpublished data). The atmospheric artifacts typically ranged about $\pm 5$ cm at New Orleans (Kwoun and Lu, unpublished data). The atmospheric delays that hamper InSAR accuracy can potentially be lessened by routinely estimating water-vapor content using a high-resolution weather model, continuous global positioning system network, or other satellite sensors such as the Moderate Resolution Imaging Spectroradiometer, Advanced Spaceborne Thermal Emission and Reflection Radiometer, and European Medium Resolution Imaging Spectrometer [42], [43].

Converting relative water-level change to absolute water-level change is challenging. Under some extreme and rare circumstances, radar backscattering intensities can be used to relate to the water-level height to resolve the phase ambiguities in the InSAR images [41]. Over our study site, exploring radar backscattering intensity did not reveal any correlation with water-level changes. Not all gauge stations can be used to help resolve the phase ambiguity of interferometric measurements. Gauge stations may be located on rivers and canals (for easy access and operation) where water-level changes may be independent of water-level changes at adjacent wetlands measured from InSAR. The satellite radar altimeters have too coarse spatial resolution to be useful to gauge the InSAR-derived water-level change. The ICESat data [44], with a spatial resolution of about 70 m, has the potential to provide estimates on absolute water-level change. Because of the phase ambiguities in the InSAR images, it is also impossible to establish water-level change time series using a multi-interferogram processing technique such as persistent scatterer InSAR [45], [46].

A more feasible solution is to include water-level measurements from a radar altimeter with adequate spatial resolution and vertical accuracy, such as the Water And Terrestrial Elevation Recovery (WATER) satellite mission [47], [48]. WATER is a Ka-band (Ka-band, $\lambda = 0.86$ cm) dual-antenna 200-MHz bandwidth system (0.75-m-range resolution) radar interferometer which can achieve centimeter-level height accuracy at tens of meters spatial resolution. A similar system will not only provide temporal and spatial variations of water-level height but also provide measurements to facilitate the use of InSAR measurements over wetlands from other satellite radar

imagery. Optimized radar images with short repeat-pass acquisitions from multiple satellite sensors, combined with available ground-based gauge readings, will improve the characterization of surface water hydraulics, hydrological modeling predictions, and the assessment of future flood events over wetlands.

## ACKNOWLEDGMENT

ERS-1/ERS-2 SAR images are copyright 1992–1998 European Space Agency (ESA) and were provided by ESA via the Category-1 Project 2853. Radarsat-1 images are copyright 2002–2004 Canadian Space Agency and were provided by the Alaska Satellite Facility (ASF). The authors would like to thank ASF and ESA for their support in programming SAR data acquisitions and delivering data timely. The authors would also like to thank C. Swarzenski (USGS) for providing them the water-level readings at the gauge stations used in this paper, and E. Ramsey, S. Faulkner, and J. Barras (all from USGS) for helpful discussion regarding the wetland characteristics over the study area. This research was supported by funding from the USGS Director Venture Capital Fund, USGS Eastern Region Venture Capital Fund, USGS Land Remote Sensing Program, NASA Solid Earth & Natural Hazards Program (SENH-0000-0229), and USGS Contract O3CRCN0001.

## REFERENCES

[1] T. Dunne, L. Mertes, R. Meade, J. Richey, and B. Forsberg, "Exchanges of sediment between the flood plain and channel of the Amazon River in Brazil," *GSA Bull.*, vol. 110, no. 4, pp. 450–467, Apr. 1998.

[2] J. Melack and B. Forsberg, "Biogeochemistry of Amazon floodplain lakes and associated wetlands," in *Biogeochemistry of the Amazon Basin and its Role in a Changing World,* M. McClain *et al.,* Eds. New York: Oxford Univ. Press, 2000.

[3] C. Prigent, E. Matthews, F. Aires, and W. Rossow, "Remote sensing of global wetland dynamics with multiple satellite data sets," *Geophys. Res. Lett.*, vol. 28, no. 24, pp. 4631–4634, Dec. 2001.

[4] D. Alsdorf *et al.*, "The need for global, satellite-based observations of terrestrial surface waters," *EOS Trans. AGU*, vol. 84, no. 29, pp. 269–276, 2003.

[5] M. Coe, "A linked global model of terrestrial hydrologic processes: Simulation of the modern rivers, lakes, and wetlands," *J. Geophys. Res.*, vol. 103, no. D8, pp. 8885–8899, 1998.

[6] L. Bourgeau-Chavez, K. Smith, S. Brunzell, E. Kasischke, E. Romanowicz, and C. Richardson, "Remote monitoring of regional inundation patterns and hydroperiod in the greater Everglades using synthetic aperture radar," *Wetlands*, vol. 25, no. 1, pp. 176–191, Mar. 2005.

[7] E. Kasischke, K. B. Smith, L. L. Bourgeau-Chavez, E. A. Romanowicz, S. M. Brunzell, and C. J. Richardson, "Effects of seasonal hydrologic patterns in south Florida wetlands on radar backscatter measured from ERS-2 SAR imagery," *Remote Sens. Environ.*, vol. 88, no. 4, pp. 423–441, Dec. 2003.

[8] L. Kiage *et al.*, "Applications of Radarsat-1 synthetic aperture radar imagery to assess hurricane-related flooding of coastal Louisiana," *Int. J. Remote Sens.*, vol. 26, no. 24, pp. 5359–5380, Dec. 2005.

[9] R. Rykhus, Z. Lu, and B. Jones, "Satellite imagery maps Hurricane Katrina induced flooding and oil slicks," *EOS Trans. AGU*, vol. 86, no. 41, pp. 381–382, Oct. 2005.

[10] O. Kwoun and Z. Lu, "Multi-temporal Radarsat-1 and ERS backscattering signatures of coastal wetlands at southeastern Louisiana," *Photogramm. Eng. Remote Sens. Environ.*, 2008. to be published.

[11] D. Massonnet and K. Feigl, "Radar interferometry and its application to changes in the Earth's surface," *Rev. Geophys.*, vol. 36, no. 4, pp. 441–500, 1998.

[12] P. Rosen, S. Hensley, I. R. Joughin, F. K. Li, S. N. Madsen, E. Rodriguez, and R. M. Goldstein, "Synthetic aperture radar interferometry," *Proc. IEEE*, vol. 88, no. 3, pp. 333–380, Mar. 2000.

[13] D. Alsdorf, J. Melack, T. Dunne, L. Mertes, L. Hess, and L. Smith, "Interferometric radar measurements of water level changes on the Amazon flood plain," *Nature*, vol. 404, no. 6774, pp. 174–177, Mar. 2000.

[14] D. Alsdorf, C. Birkett, T. Dunne, J. Melack, and L. Hess, "Water level changes in a large Amazon lake measured with spaceborne radar interferometry and altimetry," *Geophys. Res. Lett.*, vol. 28, no. 14, pp. 2671–2674, Jul. 2001.

[15] S. Wdowinski, F. Amelung, F. Miralles-Wilhelm, T. Dixon, and R. Carande, "Space-based measurements of sheet-flow characteristics in the Everglades wetland, Florida," *Geophys. Res. Lett.*, vol. 31, no. 15, p. L15 503, Aug. 2004. DOI:10.1029/2004GL020383.

[16] Z. Lu, M. Crane, O. Kwoun, C. Wells, C. Swarzenski, and R. Rykhus, "C-band radar observes water level change in swamp forests," *EOS Trans. AGU*, vol. 86, no. 14, pp. 141–144, 2005.

[17] J. Richards, P. Woodgate, and A. Skidmore, "An explanation of enhanced radar backscattering from flooded forests," *Int. J. Remote Sens.*, vol. 8, no. 7, pp. 1093–1100, 1987.

[18] A. Beaudoin *et al.*, "Retrieval of forest biomass from SAR data," *Int. J. Remote Sens.*, vol. 15, no. 14, pp. 2777–2796, 1994.

[19] L. Hess, J. Melack, S. Filoso, and Y. Wang, "Delineation of inundated area and vegetation along the Amazon floodplain with SIR-C synthetic aperture radar," *IEEE Trans. Geosci. Remote Sens.*, vol. 33, no. 4, pp. 896–904, Jul. 1995.

[20] Y. Wang, L. Hess, S. Filoso, and J. Melack, "Understanding the radar backscattering from flooded and nonflooded Amazonian forests: Results from canopy backscatter modeling," *Remote Sens. Environ.*, vol. 54, no. 3, pp. 324–332, 1995.

[21] F. Ulaby, R. K. Moore, and A. K. Fung, "Radar remote sensing and surface scattering and emission theory," in *Microwave Remote Sensing: Active and Passive*, vol. 2. Reading, MA: Addison-Wesley, 1982.

[22] E. Ramsey, III, "Radar remote sensing of wetlands," in *Remote Sensing Change Detection*, R. S. Lunetta and C. D. Elvidge, Eds. Chelsea, MI: Ann Arbor, 1999, pp. 211–243.

[23] G. Sun, "Radar backscattering modeling of coniferous forest canopies," Ph.D. dissertation, Univ. California, Santa Barbara, CA, 1990.

[24] J. Hagberg, L. Ulander, and J. Askne, "Repeat-pass SAR interferometry over forested terrain," *IEEE Trans. Geosci. Remote Sens.*, vol. 33, no. 2, pp. 331–340, Mar. 1995.

[25] U. Wegmüller and C. Werner, "Retrieval of vegetation parameters with SAR interferometry," *IEEE Trans. Geosci. Remote Sens.*, vol. 35, no. 1, pp. 18–24, Jan. 1997.

[26] E. Ramsey, III, Z. Lu, A. Rangoonwala, and R. Rykhus, "Multiple baseline radar interferometry applied to coastal land cover classification and change analyses," *GIScience Remote Sens.*, vol. 43, no. 4, pp. 283–309, Oct.–Dec. 2006.

[27] H. Zebker and J. Villasenor, "Decorrelation in interferometric radar echoes," *IEEE Trans. Geosci. Remote Sens.*, vol. 30, no. 5, pp. 950–959, Sep. 1992.

[28] Z. Lu and J. Freymueller, "Synthetic aperture radar interferometry coherence analysis over Katmai volcano group, Alaska," *J. Geophys. Res.*, vol. 103, no. B12, pp. 29 887–29 894, Dec. 1998.

[29] F. Gatelli, A. Guarnieri, F. Parizzi, P. Pasquali, C. Prati, and F. Rocca, "The wavenumber shift in SAR interferometry," *IEEE Trans. Geosci. Remote Sens.*, vol. 32, no. 4, pp. 855–865, Jul. 1994.

[30] U.S. Army Corps of Engineers (USACE), *Louisiana Ecosystem Restoration Study: Louisiana Coastal Area (LCA)*, 2004. [Online]. Available: http://www.lca.gov/final_report.aspx

[31] S. Nelson, P. A. Soranno, and J. Qi, "Land-cover change in upper Barataria Basin estuary, Louisiana, 1972–1992: Increase in wetland area," *Environ. Manage.*, vol. 29, no. 5, pp. 716–727, 2002.

[32] The Louisiana Coastal Wetlands Conservation and Restoration Task Force and The Wetlands Conservation and Restoration Authority (LCWCRTF/WCRA), *Coast 2050: Toward a sustainable Coastal Louisiana*, 1998, Baton Rouge, LA: Louisiana Dept. Nat. Resources.

[33] R. Scharroo and P. Visser, "Precise orbit determination and gravity field improvement for the ERS satellites," *J. Geophys. Res.*, vol. 103, no. C4, pp. 8113–8127, 1998.

[34] R. Abdelfattah and J.-M. Nicolas, "Interferometric SAR coherence magnitude estimation using second kind statistics," *IEEE Trans. Geosci. Remote Sens.*, vol. 44, no. 7, pp. 1942–1953, Jul. 2006.

[35] R. Goldstein and C. L. Werner, "Radar interferogram filtering for geophysical applications," *Geophys. Res. Lett.*, vol. 25, no. 21, pp. 4035–4038, 1998.

[36] M. Costantini, "A novel phase unwrapping method based on network programming," *IEEE Trans. Geosci. Remote Sens.*, vol. 36, no. 3, pp. 813–821, May 1998.

[37] R. Goldstein, H. Zebker, and C. Werner, "Satellite radar interferometry: Two-dimensional phase unwrapping," *Radio Sci.*, vol. 23, no. 4, pp. 713–720, Jul./Aug. 1988.
[38] J. Lee, M. Grunes, and E. Pottier, "Quantitative comparison of classification capability: Fully polarimetric versus dual and single-polarisation SAR," *IEEE Trans. Geosci. Remote Sens.*, vol. 39, no. 11, pp. 2343–2351, Nov. 2001.
[39] M. Santoro, J. Askne, U. Wegmuller, and C. Werner, "Observations, modeling, and applications of ERS-ENVISAT coherence over land surfaces," *IEEE Trans. Geosci. Remote Sens.*, vol. 45, no. 8, pp. 2600–2611, Aug. 2007.
[40] F. Grings *et al.*, "Monitoring flood condition in marshes using EM models and Envisat ASAR observations," *IEEE Trans. Geosci. Remote Sens.*, vol. 44, no. 4, pp. 936–942, Apr. 2006.
[41] S. Kim, S. Hong, and J. Won, "An application of L-band synthetic aperture radar to tide height measurement," *IEEE Trans. Geosci. Remote Sens.*, vol. 43, no. 7, pp. 1478–1482, Jul. 2005.
[42] Z. Li, J.-P. Muller, P. Cross, and E. Fielding, "Interferometric synthetic aperture radar (InSAR) atmospheric correction: GPS, Moderate Resolution Imaging Spectroradiometer (MODIS), and InSAR integration," *J. Geophys. Res.*, vol. 110, no. B3, p. B03 410, 2005. DOI:10.1029/2004JB003446.
[43] J. Foster *et al.*, "Mitigating atmospheric noise for InSAR using a high-resolution weather model," *Geophys. Res. Lett.*, vol. 33, no. 16, p. L16 304, 2006. DOI:10.1029/2006GL026781.
[44] L. Magruder, B. Schutz, and E. Silverberg, "Laser pointing angle and time of measurement verification of the ICESat laser altimeter using a ground-based electro-optical detection system," *J. Geod.*, vol. 77, no. 3/4, pp. 148–154, 2003.
[45] A. Ferretti, C. Prati, and F. Rocca, "Permanent scatterers in SAR interferometry," *IEEE Trans. Geosci. Remote Sens.*, vol. 39, no. 1, pp. 8–20, Jan. 2001.
[46] A. Hooper, H. Zebker, P. Segall, and B. Kampes, "A new method for measuring deformation on volcanoes and other natural terrains using InSAR persistent scatterers," *Geophys. Res. Lett.*, vol. 31, no. 23, p. L23 611, Dec. 2004. DOI:10.1029/2004GL021737.
[47] D. Alsdorf and E. Rodriguez, *WatER: The Water Elevation Recovery Satellite Mission, First Mission Document for the WatER Mission*, 2005. [Online]. Available: http://www.geology.ohio-state.edu/water/publications.php
[48] D. Alsdorf, E. Rodríguez, and D. Lettenmaier, "Measuring surface water from space," *Rev. Geophys.*, vol. 45, no. 2, p. RG2 002, Dec. 2007. DOI:10.1029/2006RG000197.

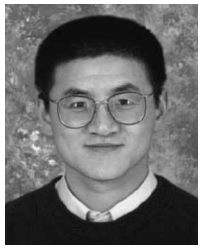

**Zhong Lu** (S'96–A'97–M'97–SM'07) received the M.S. degree from Beijing University, Beijing, China, in 1992, and the Ph.D. degree from the University of Alaska Fairbanks, Fairbanks, in 1996.

He is currently with the U.S. Geological Survey (USGS), Earth Resources Observation and Science Center and Cascades Volcano Observatory, Vancouver, WA, as a Physical Scientist. He is a Principal Investigator of projects funded by NASA, the European Space Agency, Japan Aerospace Exploration Agency, German Space Agency, and USGS on the study of land surface deformation using satellite InSAR imagery. His research interests include technique developments of SAR, InSAR, and persistent scatterer InSAR processing, and their applications on natural hazards monitoring and natural resources management.

Dr. Lu has been a committee member of the International User Team for Radarsat-C SAR Constellations, the U.S. Interagency Working Group on Orbital InSAR, the GeoEarthscope InSAR User Working Group, and NASA's Alaska Satellite Facility User Working Group. He was the recipient of the 2001 Raytheon Distinguished Level Award for Excellence in Technology and the 1999 Jerald J. Cook Memorial Award.

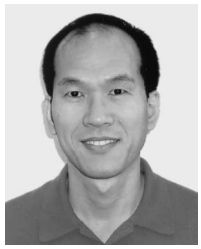

**Oh-ig Kwoun** received the M.S. degree from the Korea Advanced Institute of Science and Technology, Daejeon, in 1985.

He was trained for SAR and InSAR applications during his postgraduate study at the University of Texas, Austin. He then worked for Raytheon to support the SAR/ScanSAR data processing software system of the Alaska Satellite Facility. Since 2003, he has been with the Science Applications International Corporation, contractor to the U.S. Geological Survey (USGS) Center for Earth Resources Observation and Science, Sioux Falls, SD, to conduct SAR and InSAR applications research and to automate the InSAR data processing chain. His research interests include SAR backscatter analysis, differential InSAR, persistent scatterer InSAR, radar signal processing, and remote sensing image processing techniques.